Atomic photoionization in combined intense XUV free-electron and infrared laser fields

2012 New J. Phys. 14 043008

(http://iopscience.iop.org/1367-2630/14/4/043008)

New Journal of Physics
The open-access journal for physics

Atomic photoionization in combined intense XUV free-electron and infrared laser fields

P Radcliffe[1], M Arbeiter[2], W B Li[3], S Düsterer[4], H Redlin[4], P Hayden[5], P Hough[5], V Richardson[5], J T Costello[5], T Fennel[2] and M Meyer[1,6]

[1] European XFEL GmbH, Albert-Einstein-Ring 19, D-22761 Hamburg, Germany
[2] Universität Rostock, Institut für Physik, Universitätsplatz 3, D-18051 Rostock, Germany
[3] Institute of Precision Optical Engineering, Department of Physics, Tongji University, 1239 SiPing Road, Shanghai 200092, China
[4] HASYLAB at DESY, Notkestrasse 85, D-22607 Hamburg, Germany
[5] National Center for Plasma Science and Technology and School of Physical Sciences, Dublin City University, Dublin, Ireland
E-mail: michael.meyer@xfel.eu

New Journal of Physics **14** (2012) 043008 (12pp)
Received 17 November 2011
Published 11 April 2012
Online at http://www.njp.org/
doi:10.1088/1367-2630/14/4/043008

Abstract. We present a systematic study of the photoionization of noble gas atoms exposed simultaneously to ultrashort (20 fs) monochromatic (1–2% spectral width) extreme ultraviolet (XUV) radiation from the Free-electron Laser in Hamburg (FLASH) and to intense synchronized near-infrared (NIR) laser pulses with intensities up to about 10^{13} W cm^{-2}. Already at modest intensities of the NIR dressing field, the XUV-induced photoionization lines are split into a sequence of peaks due to the emission or absorption of several additional infrared photons. We observed a plateau-shaped envelope of the resulting sequence of sidebands that broadens with increasing intensity of the NIR dressing field. All individual lines of the nonlinear two-color ionization process are Stark-shifted, reflecting the effective intensity of the NIR field. The intensity-dependent cut-off energies of the sideband plateau are in good agreement with a classical model. The detailed structure of the two-color spectra, including the formation of individual sidebands, the Stark shifts and the contributions beyond the

[6] Author to whom any correspondence should be addressed.

classical cut-off, however, requires a fully quantum mechanical description, as is demonstrated with time-dependent quantum calculations in single-active electron approximation.

Contents

1. Introduction

The development of high-power femtosecond lasers in the near-infrared (NIR) spectral range has uncovered a rich vein of non-perturbative, multi-photon phenomena in the interaction of atoms with coherent light. It is in the strong-field region around $10^{14}\,\mathrm{W\,cm^{-2}}$ that such a behavior gives rise to above threshold ionization (ATI), high-harmonic generation (HHG) and attosecond pulse generation [1–4]. For example, short-wavelength attosecond pulses, combined with their own generating NIR radiation, open up unique possibilities to access the ultra-fast dynamics of electronic relaxation [5]. A new class of experiments has become feasible with the advent of short-wavelength free-electron lasers (FEL), providing ultrashort (20 fs) and intense pulses (10^{13} photons per pulse) from the extreme ultraviolet (XUV) to the x-ray regime within a narrow spectral width (1–2%) combined with tunability of the photon energy [6]. In particular for experiments on two-color (XUV + NIR) multi-photon processes [7], it was shown that these FEL characteristics enabled investigations free from undesirable interference effects, which often complicate the analysis of spectra recorded with HHG sources.

A key feature of XUV + NIR excitation is that electrons can be born into the low-frequency field with high kinetic energy. Hence, for a given NIR laser intensity, the probability of high-order ATI processes is much higher than that at low kinetic energies, i.e. multi-photon processes can already be observed at much lower dressing fields. In the case of one-color (NIR) ATI, the required NIR laser intensities are often close to the onset of tunnel ionization, which starts to radically alter the profile of the electron spectrum, changing it from a sequence of discrete photolines to a continuum-like character [8]. In this work, we make use of the high initial kinetic energy of the photoelectrons to produce and systematically investigate two-color ATI processes in the strong-field regime as a function of NIR intensity while retaining the multi-photon character of the photoionization process.

An illustration of the two-color laser–atom interaction is given in figure 1 together with the corresponding electron spectra simulated using the strong field approximation (atomic potential neglected). The examples shown for different XUV pulse durations represent the two limiting cases.

First, for ultrashort (attosecond) XUV laser pulses (figure 1(a)), the XUV pulses are much shorter than one optical cycle of the NIR dressing field ($\tau_{\mathrm{FWHM}}^{\mathrm{XUV}} \ll T_{\mathrm{NIR}}$). The red line indicates the momentum shift of XUV photoelectrons due to the vector potential

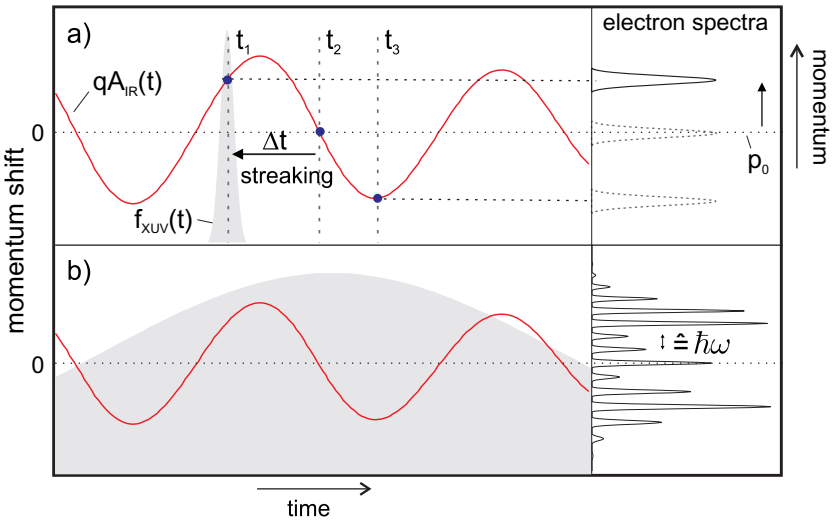

Figure 1. Simulated electron spectra for two-color photoemission from neon atoms for two different XUV pulse durations: (a) $\tau_{\mathrm{fwhm}}^{XUV} \ll T_{\mathrm{NIR}}$ and (b) $\tau_{\mathrm{fwhm}}^{XUV} \gg T_{\mathrm{NIR}}$; red lines represent the momentum shift due to the vector potential of the NIR field and gray-shaded areas indicate the XUV pulse envelope. The electron spectra show the momentum shift with respect to XUV photoelectrons without dressing field (unshifted initial momentum p_0).

$A_{\mathrm{NIR}}(t) = -\frac{E_0}{\omega_{\mathrm{NIR}}} \sin(\omega_{\mathrm{NIR}} t)$ of the NIR field $E(t) = E_0 \cos(\omega_{\mathrm{NIR}} t)$, where ω_{NIR} and E_0 are the angular frequency and the field amplitude of the NIR pulse. The gray-shaded area indicates the XUV laser intensity envelope, i.e. the temporal rate for electron release. In a simplified model, the final energy can be deduced by assuming classical motion of the XUV photoelectron in the NIR field. The final drift momentum reads $p_{\mathrm{f}} = p_0 + q A_{\mathrm{NIR}}(t_0)$, where p_0 and q are the initial momentum and charge of the electron, respectively, and the second term on the right-hand side describes the shift induced by the dressing field. Hence the final electron kinetic energy is a clear fingerprint of the vector potential at the instant of birth (see the three different birth times t_1, t_2 and t_3 in figure 1(a)). By controlling the delay time and thus streaking the moment of photoionization, it is possible to directly measure lightwaves of ultrashort few-cycle laser pulses [9, 10].

In the second scenario depicted in figure 1(b), photoionization takes place within multiples of laser periods ($\tau_{\mathrm{FWHM}}^{\mathrm{XUV}} \gg T_{\mathrm{NIR}}$) and many interfering pathways have to be taken into account for the ejected electron. As a result, the electron spectrum is strongly modulated by the so-called sideband lines, which are separated from each other by precisely the NIR photon energy. The accurate theoretical description of the process is based on quantum mechanical concepts, i.e. solving the time-dependent Schrödinger equation (TDSE). Due to the complexity of the calculations, simplified models, such as the soft-photon approximation [11] or a classical model, sometimes also referred to as Simpleman's model [12], were used. These models provide a useful description of some general features, but have clear limitations when one is aiming at a detailed study of the observed phenomena. Note that for intermediate cases, where $\tau_{\mathrm{FWHM}}^{\mathrm{XUV}} \approx T_{\mathrm{NIR}}$, electrons are emitted within about one period of the NIR-laser field and the electron spectra are characterized by more complex structures, as discussed in detail by Kazansky *et al* [13] and observed experimentally recently [14].

In all cases, the observed features in the electron spectrum depend strongly on the NIR laser intensity and are thus sensitive to the temporal and spatial overlap of the two pulses. Hence, two-color atomic photoemission offers a route to precisely analyze laser pulse characteristics. By making use of the streaking regime, the arrival time and the temporal profile of the XUV pulses from the Free-electron Laser in Hamburg (FLASH) were measured with a temporal resolution of better than 10 fs [10], when combining the XUV and THz pulses generated in the same linear accelerator. Measurements were made in the sideband regime to estimate the overall temporal resolution for pump–probe experiments at FLASH (including the large temporal jitter) with a 50 fs resolution [15] and to determine the pulse duration of the x-ray pulses at the Linac Coherent Light Source [16] with a precision of about 20 fs, respectively. In our experiments the FEL pulses (20 fs) are much longer than the optical cycle of the 800 nm dressing field (2.6 fs), so the conditions sketched in figure 1(b) are applicable, leading to characteristic ATI (sideband) features in the electron spectra. Importantly, with this two-color scheme we can analyze if the nonlinear photoionization process (sideband formation) enters the non-perturbative regime (appearance of cut-offs in the sideband plateau), i.e. the applicability and limits of the classical model can be discussed. Furthermore, we show that the high-order two-color photoionization produces a tail of sidebands well beyond the classical cut-off expected within the streaking regime.

The rest of the paper is structured as follows. The experimental details together with electron spectra as exemplars measured on atomic helium are given in section 2. A detailed analysis of two-color photoemission is performed in section 3 for the closed-shell atom neon as a function of NIR intensity. Therein the sideband-averaged features of the experimental electron spectra are compared to the predictions of the classical theory, whereas purely quantum mechanical features are discussed in comparison to the TDSE results.

2. Experiment

The experiments were performed at the beamline BL2 of FLASH, using a synchronized NIR laser system [17, 18]. The FEL and the NIR-laser were introduced into the experimental chamber in collinear geometry, where they intersected an effusive gas jet. The chamber comprises a magnetic bottle electron spectrometer (MBES), in-vacuum NIR optics as well as various beam diagnostics [19]. The photoelectrons produced by the interaction of the rare gas with the XUV beam are analyzed by the MBES with an angular acceptance close to 4π at electron kinetic energies between 15 and 100 eV. The resulting single-shot capability of the MBES is a necessary prerequisite for experiments with the strongly varying temporal and spatial beam conditions inherent to FEL radiation. In particular, the effective NIR intensity fluctuates due to the temporal and spatial jitter between the FEL and NIR pulses and has to be extracted from the single-shot data by post analysis. Before entering the time-of-flight analyzer the electrons can be slowed down to a fraction of their initial kinetic energy by means of a retarding field section, situated at a distance of about 60 mm from the interaction region, making an overall energy resolution of the order of less than 1% possible. Although the application of a retardation potential (U_{Ret}) results in an increase of the spectral resolution, it leads also to a decrease of transmission for electrons with low nominal kinetic energy, i.e. initial kinetic energy minus eU_{Ret}, of less than about 10 eV. This region in the electron spectrum will therefore not be included in the quantitative discussion of the results.

The general performance of the MBES is briefly demonstrated in figure 2, which shows the main features of the electron spectrum recorded after exposure of He atoms to XUV pulses with

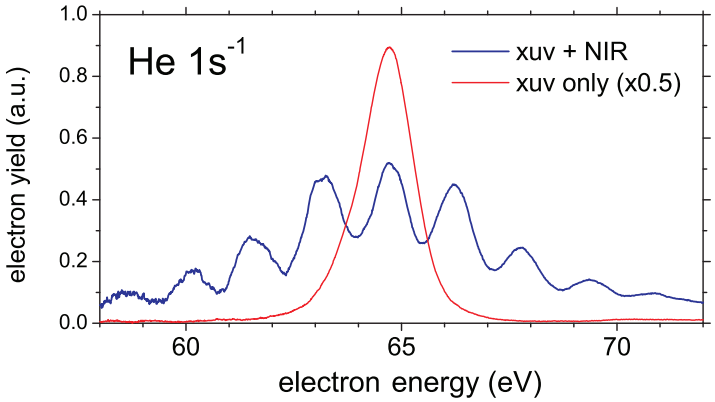

Figure 2. Two-color photoelectron spectrum (averaged over 250 shots) from atomic helium for illumination with synchronized XUV (13.9 nm) and NIR (800 nm) laser pulses showing four sidebands on either side of the main He $1s^{-1}$ line. The corresponding XUV-only spectrum recorded at $\hbar\omega_{\mathrm{XUV}} = 89.2\,\mathrm{eV}$ is shown for comparison ($U_{\mathrm{Ret}} = -50\mathrm{V}$).

a mean photon energy of 89.2 eV and NIR pulses of 1.55 eV. The undressed He $1s^{-1}$ photoline at 64.6 eV is shown for comparison. After averaging over 250 shots the line profile is well represented by a Gaussian fit of 1.5 eV full-width at half-maximum (FWHM). This value is mainly determined by the natural bandwidth of FLASH, which is of the order of 1–2% [20]. The spectrum recorded at full temporal and spatial overlap demonstrates the characteristic sideband distribution consisting of one central line corresponding to the direct 1s photoelectron line, accompanied by a nearly symmetric spread of low- and high-energy sidebands. The growth of up to four sidebands is matched by a corresponding decrease of the central line; that is, the total electron yield remains constant, as the NIR field does not contribute to the primary ionization process. We note that the laser intensity required to create the sideband features in figure 2, i.e. with ionizing photons of 13.9 nm wavelength, is $8 \times 10^{11}\,\mathrm{W\,cm^{-2}}$, which is significantly lower than the minimum intensity required for the one-color ATI process at optical wavelengths, see e.g. [8].

For the measurements presented below, FLASH was operated in single-bunch mode at a pulse repetition rate of 10 Hz and a wavelength of 26.9 nm (46 eV). The total XUV energy per pulse typically varied from 10 to 50 μJ and was monitored by a gas-based photon flux detection setup integrated into the beamline [17]. The toroidal focusing optic of BL2 produces a FEL beam diameter of 35 μm (FWHM) in the interaction volume of the MBES. The NIR-laser system consisted of a low-repetition-rate (10 Hz) Ti:sapphire setup delivering a pulse duration $\tau_{\mathrm{NIR}} = 120\,\mathrm{fs}$ (FWHM) at a central wavelength of 800 nm and a pulse energy of 1.5 mJ in the chamber. An off-axis parabola, located on the FLASH beam axis inside the experimental chamber, has a 6 mm diameter hole, through which the focused FEL beam was directed. An NIR spot of approximately 300 μm FWHM ensured good spatial overlap of the NIR and XUV beams, yielding intensities of the NIR laser in the range of $10^{13}\,\mathrm{W\,cm^{-2}}$. The spatial overlap between FLASH and the NIR laser beams was monitored by introducing a phosphor viewing screen into the region of interaction and adjusting the NIR beam steering such that both spots were overlapped. Coarse timing to a precision of 30 ps was achieved with a fast photodiode. Finally, *time zero* at the acceptance volume of the MBES was found in a cross-correlation

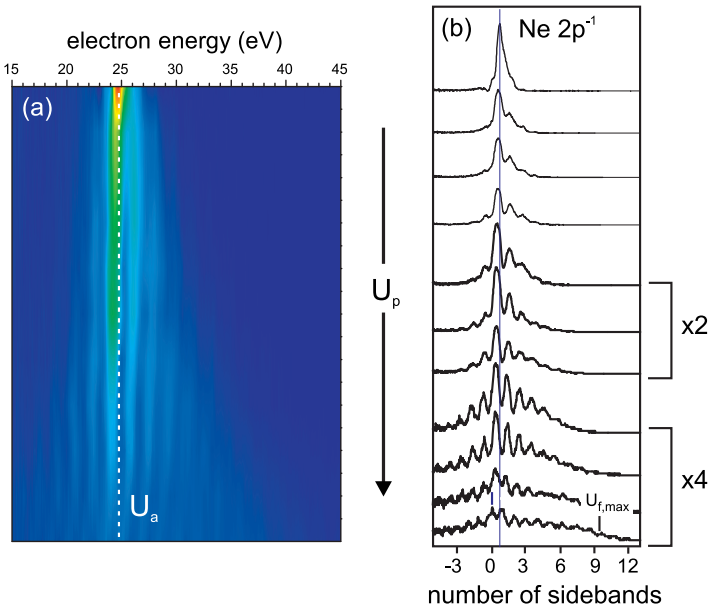

Figure 3. (a) 2D color plot representation of single-shot two-color electron spectra from atomic Ne ($\hbar\omega_{\mathrm{XUV}} = 46\,\mathrm{eV}$) recorded at the maximum temporal overlap of the XUV and NIR lasers ($U_{\mathrm{Ret}} = -12\mathrm{V}$). The data are arranged in terms of increasing ponderomotive energy (U_{p}) induced by the NIR laser field, up to $\sim 10^{13}\,\mathrm{W\,cm^{-2}}$. (b) The corresponding electron spectra from (a), highlighting the presence of the AC Stark shift on the central photoelectron line and the cut-off energy $U_{f,\mathrm{max}}$ predicted by the classical model. ($U_{f,\mathrm{max}}$ was estimated using $I_{\mathrm{NIR}} = 1.4 \times 10^{13}\,\mathrm{W\,cm^{-2}}$.)

scheme by monitoring the averaged intensity of the first sideband as a function of the NIR delay stage, see e.g. [15].

3. Results and discussion

A series of two-color single-shot electron spectra, recorded for neon at 46 eV photon energy at the maximum of the cross-correlation between the XUV and NIR beams, are displayed as a two-dimensional (2D) color plot in figure 3(a). As the spectra are normalized (constant integral) the remaining large variations in the electron energy distribution are solely due to the timing jitter of 150 fs rms of the XUV pulse with respect to the NIR pulse. The spectra are arranged in order of increasing sideband intensity, which corresponds to increasing temporal overlap or, in other words, to increasing NIR intensity experienced by the electrons at the instant of birth. The intensity of the main $2p^{-1}$ photoline, situated at 24.5 eV, decreases dramatically and sideband features at multiples of 1.55 eV develop. The first few sidebands are well resolved, whereas the higher orders which lie at high kinetic energy become blurred due to the increasing bandwidth of the MBES analyzer. The high-energy tail of the spectrum extends beyond 45 eV, corresponding to the absorption of more than 12 NIR photons. Clearly, within the cross-correlation region, the two-color ATI signal is very sensitive to the temporal overlap of the two laser beams and can be compared to the soft-photon model to determine the overlap to an accuracy of ± 20 fs [16].

Figure 3(b) shows several of the single-shot spectra in more detail, demonstrating two additional aspects of the influence of the NIR field on the photoelectrons beyond the creation of sidebands. Namely, (i) a downshift of the peaks by the ponderomotive energy at the moment of birth due to the AC Stark effect and (ii) a broadening of the peaks due to the fact that the NIR intensity is not constant during the XUV pulse. With the ponderomotive energy $U_\mathrm{p} = q^2 E_0^2/4m_e\omega_\mathrm{NIR}^2$, the observed Stark shifts of up to 1 eV correspond to peak intensities of the NIR field around $10^{13}\,\mathrm{W\,cm^{-2}}$. The characteristics of the shift and broadening depend sensitively on the delay. If the two pulses fully overlap, the infrared intensity does not change much during the XUV pulse and the extra broadening of the peaks in the electron spectrum is very small; however, the Stark shift is maximal. If the XUV pulse arrives during the rising or falling edge of the infrared pulse, where the intensity changes rapidly, the broadening is large, while the shift is minimal [21]. An inspection of the data shown in figure 3(b) highlights both trends; that is, starting from the Ne $2p^{-1}$ photoline recorded at small temporal overlap (top) the photolines in the following spectra become somewhat narrower and are progressively Stark-shifted to lower kinetic energies.

For a more detailed analysis of the intensity-dependent electron spectra, each single-shot spectrum has been sorted into one of five equally spaced bins, based on the integrated sideband signal from the high-energy side of the Ne $2p^{-1}$ photoelectron peak. After averaging the spectra in each respective group, the effective intensity of the NIR field is determined by comparison with TDSE spectra. The extracted intensities are consistent with the Stark shift of the central photoline. Figure 4 displays such group-averaged spectra for four different effective NIR intensities.

First, for a simplified theoretical analysis of the observed broadening of the sideband plateau, we employed the classical, so-called Simpleman's model [12]. Therein, the final kinetic energy U_f of an XUV photoelectron introduced into a dressing NIR field with initial kinetic energy $U_0 = \hbar\omega_\mathrm{XUV} - I_\mathrm{p}$ and angle θ_0 between the initial momentum $\mathbf{p}_0$ and the light polarization is determined fully classically. Here I_p denotes the atomic ionization potential, and light polarization along the z-axis is assumed. The model considers classical 3D motion of the released electron in the presence of the NIR field neglecting the atomic potential. The z-component of the final drift momentum $\mathbf{p}_\mathrm{f} = \mathbf{p}_0 + qA_\mathrm{NIR}(t_0)\mathbf{e}_z$ is shifted by the NIR vector potential $A_\mathrm{NIR}(t) = -\frac{E_0}{\omega_\mathrm{NIR}}\sin(\phi_0)$ at the instant of photoionization t_0 with the corresponding phase $\phi_0 = \omega_\mathrm{NIR} t_0$, leading to a final energy

$$U_\mathrm{f} = U_0 - \mathrm{sgn}(q)\sin(\phi_0)\cos(\theta_0)\sqrt{8U_0U_\mathrm{p}} + 2U_\mathrm{p}\sin^2(\phi_0). \tag{1}$$

The maximum shift occurs for $\sin\phi_0\cos\theta_0 = 1$, i.e. for initial electron momenta parallel to the polarization axis and electron release at the advantageous zero crossing of the NIR field, respectively. This yields the upper classical cut-off energy of the sidebands

$$U_\mathrm{f,max} = U_0 + \sqrt{8U_0U_\mathrm{p}} + 2U_\mathrm{p}. \tag{2}$$

A minus sign in front of the second term on the right-hand side yields the corresponding lower classical cut-off. For comparison with the experiment, electron spectra have been calculated by averaging over trajectories for all possible birth times within a full NIR cycle. The initial angular distribution of the electron momenta has been sampled according to the asymmetry parameter $\beta = 0.95$ for neon 2p at 24.4 eV excess energy [22]. Note that this classical treatment can describe neither the isolated sidebands nor the Stark shift, but provides a reference for the average structure of the two-color photoelectron spectra including the anisotropy of initial atomic photoemission.

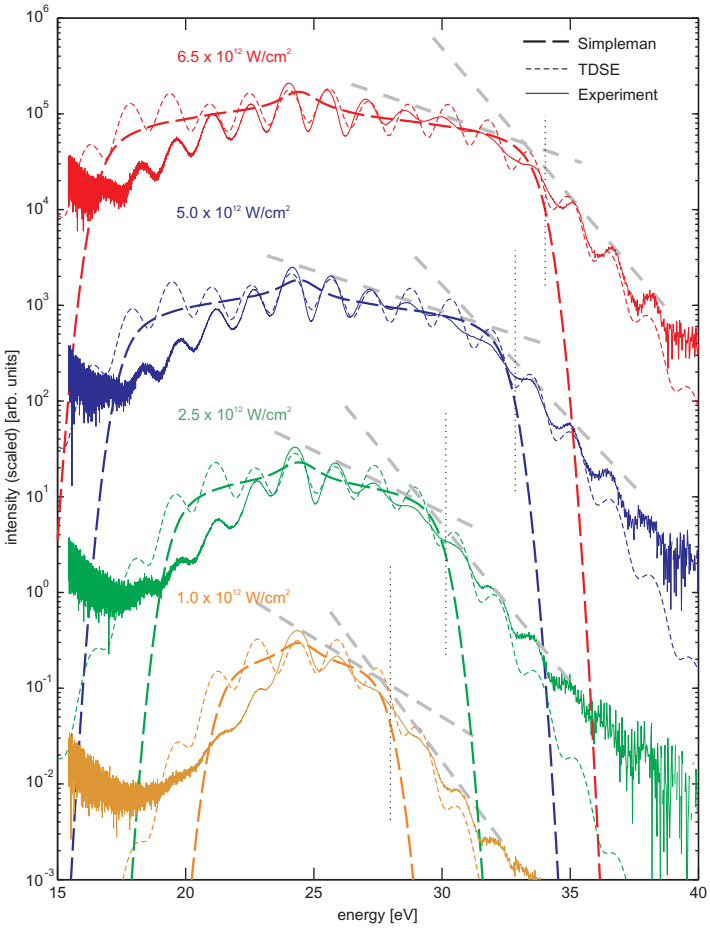

Figure 4. Experimental two-color photoelectron spectra for neon atoms at $\hbar\omega = 46\,\mathrm{eV}$ XUV excitation for four different NIR laser intensities (solid curves); $U_{\mathrm{Ret}} = -12\,\mathrm{V}$. The infrared laser intensities (as indicated) are estimated via comparison with TDSE data and are consistent with the observed AC Stark shifts. A comparison with a 3D classical model (long dashed curves) shows that the classical cut-off energy (vertical dotted lines) are in reasonable agreement with the cut-off feature in the experiment (as indicated by crossing dashed gray lines). The detailed sideband structure and the signal beyond the classical cut-off energy are well reproduced by the full TDSE results (dashed). All theoretical spectra have been broadened by convolution with a Gaussian profile $\exp(-E^2/\delta^2)$ with $\delta = 0.6\,\mathrm{eV}$ to account for the experimental spectral width of the XUV pulse. All spectra are normalized to the same integral yield.

Two conclusions can be drawn from the comparison of the experimental data with the spectra calculated within this classical model in figure 4. Firstly, near the main photoline the overall shape of the experimental sideband spectra is similar to the classical model predictions for all intensities. The reduced experimental signal towards small energies in the range $E \lesssim 20\,\mathrm{eV}$ is attributed to the decreasing detection efficiency of the spectrometer and the limited statistics for low yields. Secondly, focusing on the signal on the high-energy side, the measured spectra show clear cut-off features (shoulders) that coincide well with the very sharp cut-offs of

the classical model. This demonstrates that the classical theory provides a reliable estimate for the cut-offs in the sideband-averaged strong-field two-color photoionization spectra and thus provides a simple route for estimating the NIR laser intensity. However, although the experimental spectra exhibit a clear change in the slopes at the classical cut-off, notable signal is found well beyond this cut-off energy. These higher energies as well as the formation of the sidebands itself cannot be explained classically.

To resolve quantum effects within the two-color ATI process and, in particular, to study their impact on individual sidebands formation and the signal beyond the classical sideband cut-off, we performed time-dependent quantum mechanical simulations. To this end, we solved numerically the 3D TDSE in the single active electron approximation and atomic units

$$\mathrm{i}\frac{\partial}{\partial t}|\Psi_t\rangle = \left(-\frac{\Delta}{2} + V(\hat{r}) + [E_{\mathrm{NIR}}(t) + E_{\mathrm{XUV}}(t)]\hat{z}\right)|\Psi_t\rangle, \tag{3}$$

where E_{NIR} and E_{XUV} are the electric fields of the linearly polarized NIR and XUV laser pulses, respectively. The atomic potential is approximated by a hydrogen-like Coulomb potential $V(r) = -Z/r$ with the effective nuclear charge $Z = 2.515$ adjusted to reproduce the binding energy of the neon 2p level ($IP_{\mathrm{Ne}} = 21.5\,\mathrm{eV}$) for the initial ground state ($l = 1$). For both pulses we used a cosine squared envelope function. The electron spectra are obtained from the wavefunction at the end of the laser pulse using a window operator [23]

$$\hat{W}(E, n, \gamma) = \frac{\gamma^{2n}}{(\hat{H}_0 - E)^{2n} + \gamma^{2n}}, \tag{4}$$

where $\hat{H}_0 = -\frac{\Delta}{2} + V(\hat{r})$ is the unperturbed atomic Hamiltonian, n the order of the window function (here we used $n = 3$), and γ reflects the energy resolution of the window operator (we used $\gamma = 0.002$ au). The energy-resolved electron signal follows as $Y(E) = \langle\Psi|\hat{W}(E, n, \gamma)|\Psi\rangle$. Pulse durations (intensity FWHM) of 24 fs for the NIR pulse and 6 fs for the XUV pulse are used, leading to the same pulse duration ratio as in the experiment. Although the pulses are shorter in the simulation, we ensured that XUV photoionization proceeds over several NIR cycles. The final energy spectra are averages over the results for the three different magnetic quantum numbers $m = -1, 0, 1$ of the Ne 2p level. The calculations have been performed using the qprop code [24].

The results of the TDSE calculations are compared to the experiments in figure 4, reproducing the formation of individual sidebands in great detail. Except for the signal at low energy, which is attributed to the lowered experimental detection efficiency, the spectra are in excellent agreement with the measured spectra. In particular, also the high-energy tail beyond the classical cut-off is reproduced well in the theory, demonstrating the presence of high-order multi-photon processes in the quantum mechanical response beyond the classical limit. The remaining small deviations are attributed to the unavoidable intensity averaging introduced by the binning process in the analysis of the experimental single-shot spectra.

Having demonstrated the excellent agreement of the experimental data with TDSE results, we now return to the comparison of the classical theory to the fully quantal response on the theoretical level for a broader range of intensities and using a bandwidth-limited XUV pulse. The results are shown in figure 5. For all NIR intensities the TDSE results show strong sidebands in the electron spectrum and Stark shifts of the main photoline by the ponderomotive energy (see the right panel). Between $I_{\mathrm{NIR}} = 10^{11}$–$10^{12}\ W\,\mathrm{cm}^{-2}$ the emerging sidebands begin to form

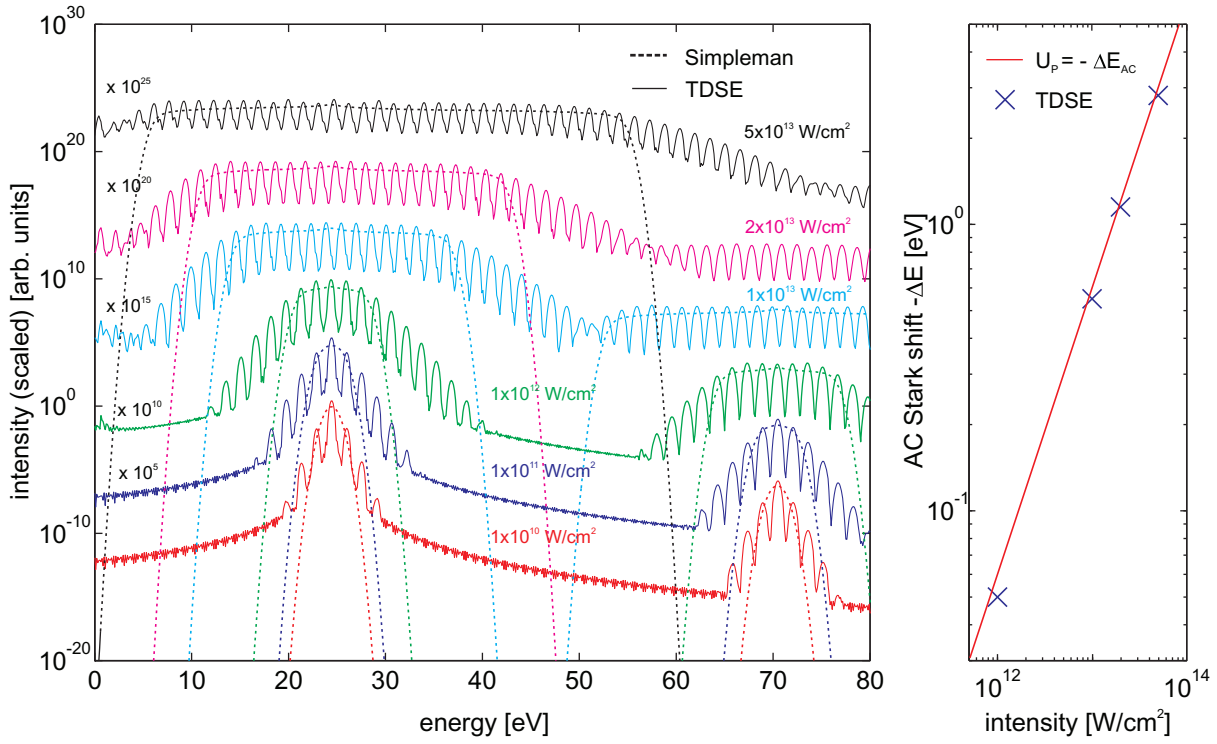

Figure 5. Left: comparison of electron spectra predicted from the classical theory (dashed lines) with TDSE results (solid lines) for a set of NIR laser intensities at constant XUV excitation ($\hbar\omega = 46\,\mathrm{eV}$ and $I = 10^{12}\,\mathrm{W\,cm^{-2}}$). The classical theory spectra for the sideband feature that corresponds to the absorption of two XUV photons (centered around $\approx 70\,\mathrm{eV}$) are shown only for the four lower intensities for clarity. Right: comparison of the AC Stark shift from TDSE simulations (crosses) to the analytical value for the NIR peak intensity $-\Delta E = U_\mathrm{P}$.

a plateau-shaped region. This feature marks the onset of non-perturbative processes, as lowest-order perturbation theory predicts a pure $I_\mathrm{NIR}^{|n|}$ scaling of the nth sideband intensity and thus only explains exponential envelopes without cut-off features. The overall increase of the width of the plateau of sidebands is similar to the prediction of the classical theory. It should be noted that the TDSE spectra also contain sideband structures resulting from two-color excitation involving the absorption of two XUV photons (signal near 70 eV) with slightly stronger intensity-dependent broadening due to the higher initial energy (see equation (1)). Also here the TDSE spectra clearly show signal beyond the classical sideband cut-off, underlining the quantum mechanical nature of the two-color ionization process. Nevertheless, the intensity-dependent position of the cut-off predicted by the classical theory at high NIR intensity is in good agreement with the simulation for both, the single- and two- XUV-photon sideband features.

From these findings several global aspects of the two-color photoemission dynamics can be readily gleaned: (i) the experimental electron spectra and TDSE calculations have shown that the sideband formation is highly sensitive to the NIR-laser intensity. The two-color spectra offer a route to characterize laser parameters, such as laser intensities, temporal shifts and spatial

overlap of the two laser fields. From the ponderomotive AC Stark shift ($-U_p$), the effective NIR-laser intensity can be easily inferred. We found maximum Stark shifts of up to 1 eV, which corresponds to a peak intensity of $I_{NIR} \lesssim 1 \times 10^{13}$ W cm^{-2}. This value is in good agreement with our measurements of the NIR parameters (i.e. focus size, energy and pulse duration). (ii) The classical cut-off energy for electron emission parallel to the laser polarization vector is found to be in good agreement with the observed shoulders of the sideband plateaus (see indications of slopes, gray lines in figure 4, providing an independent measure of the effective NIR intensity). The broadening of the sidebands provides a measure of spatial or temporal gradients of the NIR intensity. (iii) Besides the good agreement of the main features, the two-color ionization shows high-kinetic-energy contributions well above the classical cut-off energy. These reflect the importance of a fully quantum mechanical description of the two-color ionization process even in the high-intensity domain.

4. Conclusion

In conclusion, we have reported the observation of a large number of sidebands in two-color atomic photoemission, without interfering contributions between multiple quantum paths, and have made detailed comparisons with classical and quantum mechanical simulations. The intensity distribution of the sidebands and position of the peaks, determined by the ponderomotive shift, was measured for varying laser intensities and was shown to be in good agreement with both the classical and quantum models of the XUV–NIR photoionization process. While the classical approach cannot explain discrete sidebands, the overall kinetic energy distribution of the spectrum is reasonably well described. This highlights that, on average, the action of the highly nonlinear dressing field can be well described with the simplified classical picture in the non-perturbative regime.

Acknowledgments

We acknowledge the work of the scientific and technical teams at FLASH, in particular the machine operators and run coordinators. TF and MA gratefully acknowledge stimulating discussions with D Bauer, financial support from the DFG via SFB 652/2 and computer time provided by the High-Performance Computing Center for North Germany (HLRN). Support from the EU RTD project X-Ray FEL Pump-Probe HRPI-CT-1999-50009, the Science Foundation Ireland (grant no. 07/IN.1/I1771), the HEA PRTLI IV and V INSPIRE programs, IRCSET (Irish Research Council for Science, Engineering and Technology) and the France–Ireland ULYSSES program is acknowledged. WBL gratefully acknowledges financial support from the National Nature Science Foundation of China (grant no. 11075118).

References

[1] Di Mauro L F and Agostini P 1995 *Adv. At. Mol. Opt. Phys.* **35** 79
[2] Salières P, L'Huillier A, Antoine P and Lewenstein M 1999 *Adv. At. Mol. Opt. Phys.* **41** 83
[3] Kling M F and Vrakking M J J 2008 *Annu. Rev. Phys. Chem.* **59** 463
[4] Krausz F and Ivanov M 2009 *Rev. Mod. Phys.* **81** 163
[5] Drescher M *et al* 2002 *Nature* **419** 803
[6] Feldhaus J, Arthur J and Hastings J B 2005 *J. Phys. B: At. Mol. Opt. Phys.* **38** S799

[7] Meyer M, Costello J T, Düsterer S, Li W B and Radcliffe P 2010 *J. Phys. B: At. Mol. Opt. Phys.* **43** 194006
[8] Mevel E, Breger P, Trainham R, Petite G and Agostini P 1993 *Phys. Rev. Lett.* **70** 406
[9] Goulielmakis E *et al* 2004 *Science* **305** 1267
[10] Frühling U *et al* 2009 *Nature Photon* **3** 523
[11] Maquet A and Taïeb R 2007 *J. Mod. Opt.* **54** 1847
[12] Schins J M *et al* 1994 *Phys. Rev. Lett.* **73** 2180
[13] Kazansky A K, Sazhina I P and Kabachnik N M 2010 *Phys. Rev.* A **82** 033420
[14] Meyer M *et al* 2012 *Phys. Rev. Lett.* **108** 063007
[15] Radcliffe P *et al* 2007 *Appl. Phys. Lett.* **90** 131108
[16] Düsterer S *et al* 2011 *New J. Phys.* **13** 093024
[17] Tiedke K *et al* 2009 *New J. Phys.* **11** 023029
[18] Redlin H *et al* 2011 *Nucl. Instrum. Methods* A **635** 88
[19] Radcliffe P *et al* 2007 *Nucl. Instrum. Methods* A **583** 516
[20] Ackermann W *et al* 2007 *Nature Photon* **1** 336
[21] Toma E S *et al* 2000 *Phys. Rev.* A **62** 0618015
[22] Becker U and Shirley D A (ed) 1996 *VUV and Soft X-Ray Photoionization* (New York: Plenum)
[23] Kulander K C, Schafer K J and Krause J L 1992 *Atoms in Intense Laser Fields* ed M Gavrila (San Diego, CA: Academic) p 247
[24] Bauer D and Koval P 2006 *Comput. Phys. Commun.* **174** 396